Experimental estimation of the local heat transfer coefficient for thin liquid film evaporation in a capillary tube

L. Cattani, F. Bozzoli, Vincent Ayel, C. Romestant, Y. Bertin

Experimental estimation of the local heat transfer coefficient for thin liquid film evaporation in a capillary tube

L Cattani[1], F Bozzoli[1], V Ayel[2], C Romestant[2], Y Bertin[2]

[1] Department of Engineering and Architecture, University of Parma, Parma, Italy

[2] Institut Pprime, CNRS-ENSMA-Université de Poitiers, UPR 3346, 1, avenue Clément Ader, 86961 Futuroscope Chasseneuil Cedex, France

Corresponding author: luca.cattani1@unipr.it

Abstract. Two-phase heat transfer devices consisting of mini and micro tubes represent a powerfull solution to the continuous reduction of electronic components dimension and the increase of the power to dissipate. Despite many papers studied the two-phase heat transfer phenomenon in mini tubes, the great majority of them provided the outcomes with regard to the average heat transfer coefficient or Nusselt number. A technique to assess the local convective wall heat flux and heat transfer coefficient is here proposed, validated and then applied to the experimental case of the thin film evaporation in a heated capillary tube. In fact, the evaporation of the thin film of liquid plays a vital part in the two-phase heat transfer phenomena inside mini/micro-tubes. In this work this phenomenon is studied by investigating a semi-infinite slug flow. The estimation method used is represented by the inverse heat conduction problem solution in the tube wall applying the Tikhonov regularization method. The temperature distributions on the outer surface of the channel measured by an infrared camera were employed as input data of the inverse problem. The estimated heat transfer coefficient distributions confirm the available correlations in terms of average values and give an original insight of these complex phenomena by local and instantaneous quantities.

1. Introduction

One of the core contemporary issues is represented by the heat control of electronic components, since the fast and continuous reduction of chips dimension and the relentless increase of their dispelled power; it needs ground-breaking techniques that assurance the link among elevated heat transfer

performing and small size [1]. A powerful answer is constituted by two-phase heat exchange in mini and micro ducts: they accomplish with necessities for heat power rise and decrease working and fabricating charges whereas obtaining a meaningfully favourable ecological effect by lessening the quantity of material and/or of the working fluids in the devices [2]. The improvement of microdevices is establishing a demand for a deeper knowledge of microscale transport problems, thus producing global rerouting of transport studies, from macro to microscale. Considerable variations in transport physics have been described at the microscale respect to the macroscale.

There is an increasing volume of experimental analysis on two-phase heat exchange in micro-ducts. Several reviews have been published on the topic [3-5]. These works highlighted the critical issue of the cut-off from macroscale to microscale heat exchange, the different regimes that characterise the two-phase flow in microscale and the principal phenomena that rule the heat transfer behaviour of microchannels in case of two-phases processes. Usually in macroscale the nucleate boiling is considered the main heat transfer process while Jacobi and Thome [6] presented a two-zone model for the heat exchange with evaporation in microchannels which proved that the dominant contribute comes from the transitory vaporization of the narrow liquid films encircling prolonged bubbles. Chauris et al. [7] confirmed that a central part in the two-phase heat exchange in mini/micro-conduits is exerted by vaporization of the fine films of liquids surrounding vapour bubbles: the meniscus lodges a narrow quantity of liquid among the channel wall and the bubble, and the vaporization of this liquid thin layer promotes a powerful heat transfer, producing, as a consequence, an extremely important diminution of external wall temperature. Additionally, it was determined [8] that, since macroscale models are focused on the nucleate boiling and convective vaporization processes, they cannot be adopted as prediction models for the flow boiling coefficients in microchannels where the principal heat exchange contribute comes from the transient thin film evaporation. It was confirmed also by Kandlikar [9] who performed a wide investigation of the two-phase phenomena inside mini channels by the direct visualization of liquid slugs and vapour bubbles. Direct visualization provided awareness of boiling flow phenomena at this scale highlighting that the predominant flow regime is represented by the lengthened bubble flow pursued by the annular stream.

It happens also for pulsating heat pipes (PHPs): in these two-phase passive devices the fluid motion is thermally driven, and a core role is played by capillary forces. They are basically constituted by a capillary pipe bent several times to create multiple turns [10]. The pipe is partially filled with a working fluid at the liquid/vapour saturation state: thanks to surface tension effects the fluid is distributed in liquid slugs and vapour plugs. During phase-change heat transfer across menisci in PHPs, a key impact derives from the evaporation of the thin film of liquid that is deposited on part of the internal wall of the pipe [11]. This phenomenon greatly supports the movements of slugs and plugs thanks to the fast

vaporization of the extremely low thickness of liquid layer (δ, few tens of μm). Heat transfer during thin film evaporation is driven by heat conduction inside the thickness of the film. The extremely small thickness brings to elevated values of the heat transfer coefficient. They are significant in comparison to those achieved with sensible heat transfer in liquid slugs in laminar flows and vapour plugs

Therefore, the estimation of the heat transfer performance for transient thin film vaporization is of crucial significance for the thermal characterization of these device and for their design. In particular, it is fundamental not only to averagely describe this behaviour but to locally investigate the distribution of heat fluxes and heat transfer coefficient at the interface among the fluid and internal wall of the channel. For this reason, it is here proposed an experimental study of the local heat flux and heat transfer coefficient in the case of film vaporization in a capillary duct. The investigation is carried out by analysing the case of a semi-infinite slug flow in a capillary copper pipe. A powerful method to evaluate h on the inner wall of a tube relied on the solution of Inverse Heat Conduction Problem (IHCP) in the wall using as starting values the duct outer surface temperature measurements [12].

Different works are already available in the literature that provide numerical models or experimental studies to find out the heat transfer coefficient in mini or micro-ducts in presence of flow boiling.

However, almost the totality of them didn't locally estimate the heat flux but considered it as uniformly distributed on the pipe surface [5,13,14]. Moreover, in many cases the external pipe wall temperature was used instead of the internal one in the estimation of the heat transfer coefficient [14,15]. As it was shown in [16], even if it was for a single-phase flow, ignoring the conductive heat transfer taking place in the wall of the channel distorts the estimated coefficient distribution, augmenting and diminishing the minimum and the maximum local values, respectively. For this reason, the IHCP solution in the wall of the mini or micro-channel represents a very powerful tool since it permits to find the local (in space and in time) heat flux distribution and to evaluate the temperature at the internal surface of the duct that is very difficult to measure, and it is hard to find analytically for non-equilibrium problems. Consequently, it allows a more precise evaluation of the local heat transfer coefficient value and a trend that more closely characterises the physics governing the device.

Inverse heat conduction problems are not very easy to be solved: since they are normally ill-posed, the result could not be singular and should be characterised by a high sensitivity to limited changes in the starting data [17]. To manage with it, many methods were developed and here, the Tikhonov regularization technique [18] is used. Applying this method to infrared temperature measurements on the external surface of a copper capillary channel it was feasible to assess the heat fluxes of evaporation and the distribution of the local heat transfer coefficient value at the fluid to inner surface interface.

2. Experimental Setup

The experimental apparatus was specifically designed to facilitate the temperature acquisition, by thermography, on the external surface of a capillary tube containing a liquid flow followed by a long vapour bubble. A complete description of the experimental set-up can be found in [7]. The scheme of the setup is reported in figure 1: it is constituted by a capillary copper pipe characterized by a length of 0.2 m, an internal diameter of 2 mm and a wall thickness of 0.2 mm. The tube is connected to a power supply (XANTREX XDC-20-300) that allows a uniform heat generation in the wall by Joule effect.

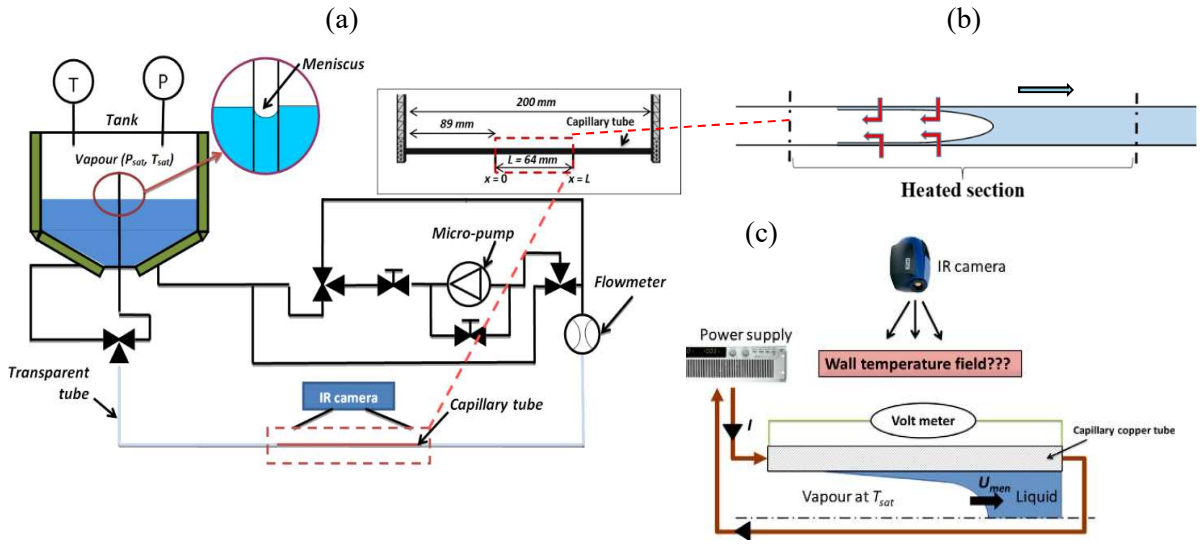

Figure 1. Scheme of: (a) the experimental loop set-up; (b) the capillary tube crossed by the liquid/vapour meniscus and (c) details of the infrared visualization window.

The external wall temperature of the copper channel was acquired by a FLIR SC7200 infrared camera that was placed perpendicularly to the channel as shown in figure 1c. The camera is characterised by a sensitivity less than 25 mK and by an accuracy of ± 1 K, as declared by manufacturer. With this experimental setup and in order to limit the viewing angle to less than ±30°, the camera measured the external temperature of a portion of the pipe of 0.064 m long. The sampled section is composed by 320 x 12 pixels that corresponds to a 0.2 x 0.2 mm^2 pixel space resolution. The whole capillary tube external surface was painted with a high emissive black paint (ε = 0.95 ±0.01).

A volumetric pump (MICROPUMP GA X21, figure 1a) provided the system with the working fluid, i.e. demineralized water whose flowrate was gauged by a Coriolis mass flowmeter (EMERSON CMFS010, accuracy of ±0.01%). The pipes circuit is characterised by an external diameter equal to 3.2 mm with a thickness of 0.4 mm, except for two transparent sections made in vinyl that are placed immediately before and after the capillary copper tube and presented 1/8 and 1/4-inch inner and external diameters, respectively. The fluid is initially contained inside a stainless-steel tank where the liquid is in thermal equilibrium with its vapour and the temperature is monitored by a thermostatically controlled

reservoir. The tank allows to monitor the fluid saturation condition by means of two K-type thermocouples, previously precisely calibrated (±0.1 K), and by a pressure transducer (UNIK5000 GE, ±80 Pa) placed in the area of the tank occupied by vapour (i.e. close to the top): it has been conceived large enough to prevent any changes in the fluid thermodynamic state during fluid flow in the loop. Adopting a classical liquid/vapour equilibrium chart it is possible to double-checking it. The pressure of the vapour is also controlled by another manometer placed upstream the heated capillary pipe.

As it possible to see from the setup scheme in figure 1 the three-way valve positioned downstream the tank allows to obtain the flow of a liquid slug terminated by a meniscus and pursued by a semi-infinite vapour bubble. The two transparent pipes allow to confirm the absence of modification of the flow and the meniscus both before and after the copper tube. Therefore, it was generated the flow of a meniscus at known velocity that divide a semi-infinite liquid slug from a semi-infinite vapour bubble. The properties of the fluid were assessed at the saturation temperature since the whole circuit is leak-tight to keep the saturation condition. The system was vacuumized before introducing the working fluid. After filling, the tank was temporally degassed in order to evacuate non condensable gases, until matching the tank measured temperature and the corresponding saturation one calculated thanks to the pressure transducer, with a 0.2 K accuracy. In addition, a K-type thermocouple placed on the external surface at the inlet section of the capillary pipe allowed the monitoring of the liquid fluid temperature.

3. Estimation Procedure

The problem is embodied by the heat conduction in the wall of a cylindrical tube. As it is shown in figure 2 the studied domain was considered as 2-D axisymmetric thanks to the fact that the temperature practically doesn't change in the angular direction. Considering these assumptions the energy balance can be written as:

$$k\nabla^2 T + q_g = \rho c_p \frac{\partial T}{\partial t} \tag{1}$$

where k is the wall thermal conductivity, ρ is the density, c_p is the specific heat, and q_g the heat power generated in the volume. The consequent boundary conditions, closed the energy balance formulation:

$$k\frac{\partial T}{\partial r} = -\frac{(T-T_{env})}{R_{env}}, \quad r = r_{ext} \tag{2}$$

which is employed on external wall and where R_{env} is the global heat-transfer resistance among the external pipe surface and the ambient that is at T_{env};

$$k\frac{\partial T}{\partial r} = q(x,t)\,, \quad r = r_{int} \tag{3}$$

which is implemented on the internal wall and where q is the local convective heat flux at the inner surface which changes with the axial coordinate x and the time t.

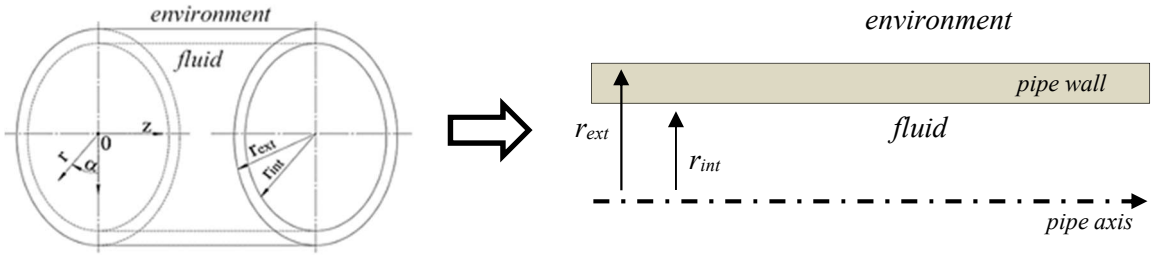

Figure 2. Geometrical domain

The q distribution is correlated to the internal convective heat transfer coefficient:

$$h(x,t) = \frac{q(x,t)}{T(t,x,r = r_{int}) - T_b} \tag{4}$$

where T_b is the bulk fluid temperature considered equal to the saturation temperature measured in the tank and checked along the line, and $T(x,r = r_{int})$ is the temperature on the inner pipe surface.

In the direct problem formulation of Eqs. (1-4), the physical properties of the wall (k, ρ and c_p), the geometry, the boundary conditions (q, T_b, T_{env}, R_{env}) are noted whereas the outer wall temperature is computed. In the inverse problem conceptualization, on the contrary, the external surface temperature field is considered as known and the heat transfer coefficient among the fluid and the inner pipe wall must be derived for specific physical properties, geometry, and boundary conditions. The heat conduction problem, according to [17,20], in the discrete domain writes as:

$$\mathbf{T} = \mathbf{X}\mathbf{q} + \mathbf{T}_{\mathbf{q=0}} \tag{5}$$

where **T** and **q** are the discrete external wall temperatures and internal wall heat flux vectors, respectively. $\mathbf{T}_{\mathbf{q=0}}$ is a invariable term that is obtained by assuming a zero heat flux vector and **X** is the sensitivity matrix. Both **X** and $\mathbf{T}_{\mathbf{q=0}}$ values, for the studied issue, could be numerically computed [12,

17,20]. In the present paper the numerical computation was performed by FEM method with Comsol Multiphysics® software. The temperature vector could be formulated as:

$$\mathbf{T}=\begin{bmatrix}\mathbf{T(1)}\\ \mathbf{T(2)}\\ \vdots\\ \mathbf{T(N)}\end{bmatrix}, \qquad \mathbf{T(i)}=\begin{bmatrix}T_1(i)\\ T_2(i)\\ \vdots\\ T_J(i)\end{bmatrix} \tag{6a, b}$$

where i indicates the i^{th} of the N time steps. The $\mathbf{T}(i)$ vector elements, presented in Eq. (6b), are the temperatures on the outer surface of the channel at various j axial spatial position (1, 2, …, J) at the i^{th} time step. The $\mathbf{q}$ vector is written as:

$$\mathbf{q}=\begin{bmatrix}\mathbf{q}(1)\\ \mathbf{q}(2)\\ \vdots\\ \mathbf{q}(N)\end{bmatrix}, \qquad \mathbf{q(i)}=\begin{bmatrix}q_1(i)\\ q_2(i)\\ \vdots\\ q_K(i)\end{bmatrix} \tag{7a, b}$$

Similarly, $\mathbf{q}(i)$ heat flux vector components are identified at various k axial positions (1, 2, …, K) at the i^{th} time step. The $\mathbf{X}$ matrix is displayed as:

$$\mathbf{X}=\begin{bmatrix}\mathbf{x}(1) & 0 & 0 & \cdots & 0\\ \mathbf{x}(2) & \mathbf{x}(1) & 0 & \cdots & 0\\ \mathbf{x}(3) & \mathbf{x}(2) & \mathbf{x}(1) & \cdots & \vdots\\ \vdots & \vdots & \vdots & & 0\\ \mathbf{x}(N) & \mathbf{x}(N-1) & & \cdots & \mathbf{x}(1)\end{bmatrix} \tag{8}$$

where:

$$\mathbf{x(i)}=\begin{bmatrix}x_{11}(i) & x_{12}(i) & \cdots & & x_{1K}(i)\\ x_{21}(i) & x_{22}(i) & \cdots & & x_{2K}(i)\\ x_{31}(i) & x_{32}(i) & \ddots & \cdots & x_{3K}(i)\\ \vdots & \vdots & & x_{jk}(i) & \vdots\\ & & & \ddots & \\ x_{J1}(i) & x_{J2}(i) & \cdots & \cdots & x_{JK}(i)\end{bmatrix}, \qquad x_{jk}(i)=\frac{\partial T(x_j,t_i)}{\partial q_k(t_1)} \tag{9a,b}$$

The assessment method is incorporated in the inverse resolution of the problem represented by Eqs. (1-4). The outer wall temperature distribution, $\mathbf{T}$, may be effortlessly calculated numerically, by considering a trial $\mathbf{q}$ distribution on the inner surface of the pipe. Under the inverse approach, the

calculated values of **T** are obligated to fit with the experimentally measured values of **Y** by adjusting the values of **q**.

The agreeing of the two temperature distributions (**T** and **Y**) can be simply assessed adopting the classical least square approach. Nevertheless, since inverse problems are ill-posed, following the least square approach doesn't produce accurate results because they are prevailed by noise, and it is necessary to adopt a regularization technique. In the present work the Tikhonov regularisation technique was used; this method [18], permits to rewrite the starting problem as a well-posed one that entail the minimisation of the subsequent goal function:

$$f(\mathbf{q})=\left\|\mathbf{Y}-\mathbf{Xq}-\mathbf{T}_{\mathbf{q}=\mathbf{0}}\right\|_2^2+\lambda^2\|\mathbf{Lq}\|_2^2 \tag{10}$$

where $\|\quad\|_2^2$ represents the squared 2-norm, λ is the regularisation factor, **L** is the derivative operator (zero-order in the present work) and $\mathbf{T}=\mathbf{Xq}-\mathbf{T}_{\mathbf{q}=\mathbf{0}}$ is the outer wall temperature distribution obtained by solving the direct problem with a known **q** distribution as boundary condition on the inner tube wall. The expression f(**q**), shown in Eq. (10), constitutes a balancing among the quality of the match and the solution steadiness. For this reason, it is very important to properly choose the regularisation parameter λ that allows to find a trade-off among the weights of the residual and solution norm. This goal could be efficiently obtained by adopting L-curve method [20] that find λ by identifying the 'corner' of the curve represented in the z,w plane:

$$\begin{cases} \boldsymbol{z_\lambda} = log\left(\left\|\boldsymbol{Y}-\boldsymbol{Xq_\lambda}-\boldsymbol{T_{q=0}}\right\|_2\right) \\ \boldsymbol{w_\lambda} = log(\|\boldsymbol{Lq_\lambda}\|_2) \\ \lambda > 0 \end{cases} \tag{11}$$

The motivation for this way to select the regularizing factor λ is related to the fact that the curve above reported is usually L-shaped, and its knee coincides to a value of λ which delivers a satisfying equilibrium among the solution and the residual norms.

After determining the **q** distribution on the inner pipe wall, it is feasible to compute the local h distribution from Eq. (4). It might be appropriately displayed in a dimensionless mode through the Nusselt number, as follows:

$$Nu = \frac{h_{\text{int}} \cdot D_{\text{int}}}{k_f} \tag{12}$$

where k_f is the thermal conductivity of the fluid at the bulk temperature.

4. Validation of the estimation procedure

As first step the estimation procedure here proposed, was validated by adopting synthetic data: adopting a defined distribution of $h(x,t)$ at the internal tube wall it was possible to obtain synthetic temperature by solving the direct problem described by Eqs. (1-4). The direct problem was solved numerically by implementing the 2D model showed in figure 2 in the COMSOL Multiphysics® environment in accordance with the parameters values of Table 1 and with a mesh characterised by $2.5 \cdot 10^3$ elements of triangular shape. The grid independence test has been carried out and the quality of the mesh was completely examined to guarantee the exactness of the numerical results (average elements quality ~ 0.984). The temperature distributions obtained from the direct problem solution were spoiled by Gaussian noise characterised by standard deviation σ in the range 0.01 - 0.5 K and adopted as starting data in the inverse problem formulation.

Table 1: Parameters adopted in the numerical validations.

q_g (W/m^3)	T_b (K)	k (W/m·K)	T_{env} (K)	R_{env} (m^2·K /W)
$5 \cdot 10^7$	317.25	401	295.65	0.1

In line with what it is expected in the real problem, the coefficient h was considered as a step function that varies both in time and space:

$$\begin{aligned} h(x,t) &= A \quad 0 < t \le t_1 + \frac{x}{\Delta x} \cdot \Delta t \\ h(x,t) &= B \quad t_1 + \frac{x}{\Delta x} \cdot \Delta t < t < t_2 \end{aligned} \tag{13}$$

where the values of the parameters A, B, Δx, Δt, t_1 and t_2 (table 2) were chosen as representative of the experimental setup and rate of change of the coefficient h both along space and time (figure 3). This state corresponds to a liquid flow followed by a long vapour bubble moving at 0.2 m/s.

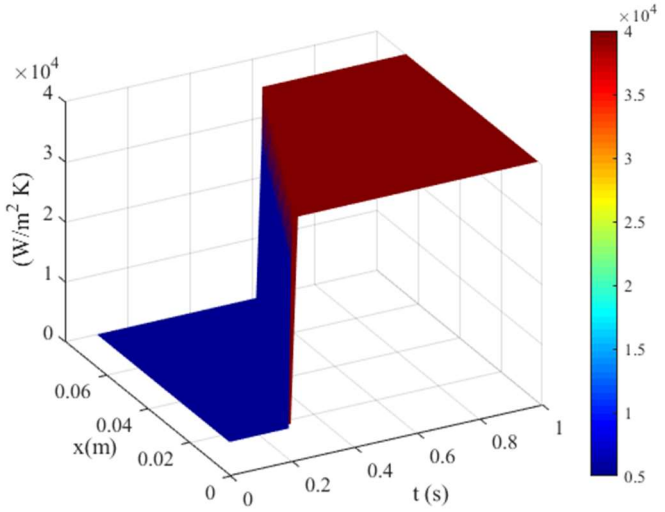

Figure 3. Synthetic convective heat transfer coefficient distribution used in the validation process.

Table 2: Parameters of the heat transfer coefficient distribution adopted in the validation procedure

A (W/m^{2}K)	B (W/m^{2}K)	Δx (m)	Δt (s)	t_1 (s)	t_2 (s)
$5 \cdot 10^3$	$4 \cdot 10^4$	0.002	0.01	0.2	1

Figure 4 reports the temperature distribution on the outer surface of the copper pipe achieved by solving the numerical model of the direct problem in Comsol Multiphysics environment. It is reported the representative case of the temperature spoiled by a random noise of $\sigma = 0.1$ K.

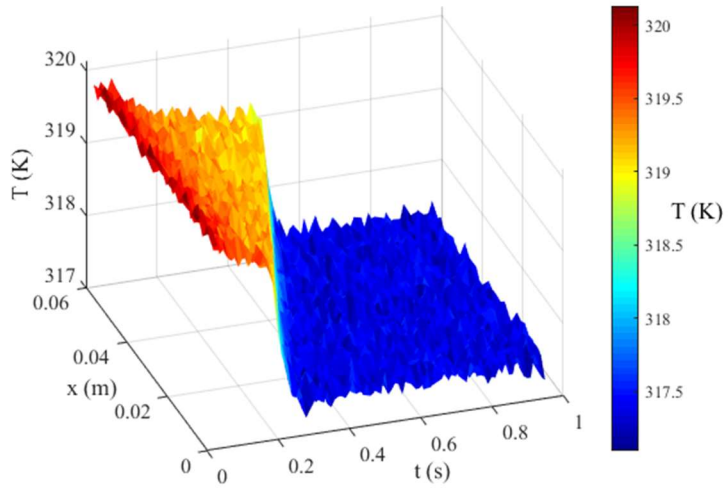

Figure 4. Synthetic T distribution on the outer wall ($\sigma = 0.1$ K).

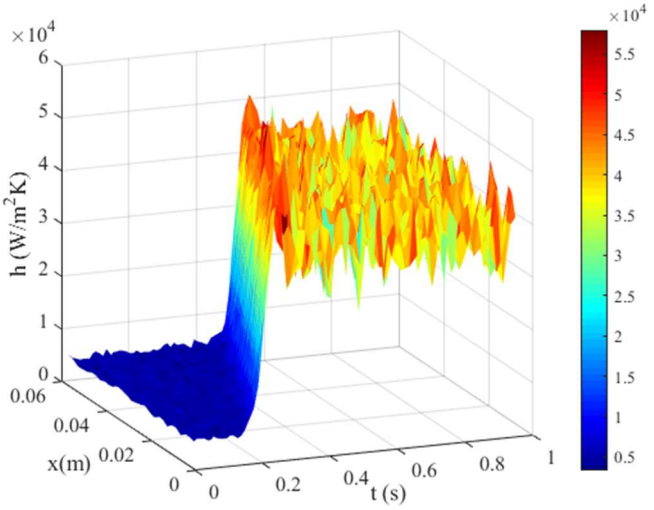

Figure 5. Reconstructed *h* distribution achieved with Tikhonov method ($\sigma = 0.1$ K).

In figure 5, the local *h* values achieved thanks to the estimation method previously explained, are shown. The proper regularization factor λ (Eq. (10)), has been determined thanks to the L-curve method [20], to be $2.0 \cdot 10^{-5}$

The *h* restored values and the original ones are contrasted in figure 6, considering the time distribution in one point (at $x = 0.04$ m, figure 6a) and the axial distribution for one instant (at t = 0.34 s, figure 6b). The restored values appropriately fit the starting local convective heat flux distribution.

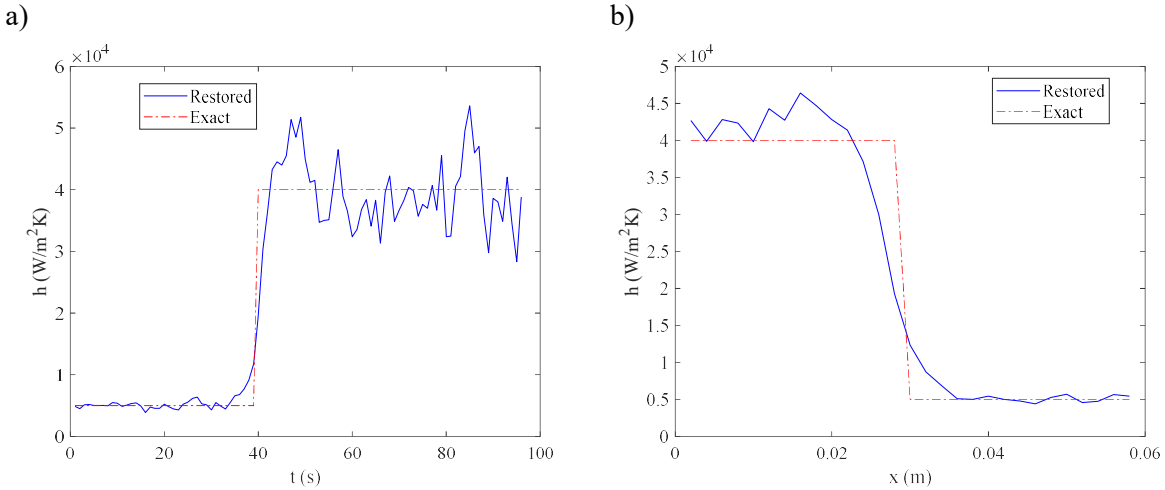

Figure 6. Exact and restored *h* (σ = 0.1 K): (a) at $x = 0.04$; (b) at $t = 0.34$ s.

Figure 7 demonstrates that the residuals between experimental (i.e. with noise) and computed temperature (i.e. obtained from IHCP solution) values are randomly distributed. It shows that the solution approach here adopted is adequate. Moreover, computing the root mean square residuals the value of 0.101K has been found: it confirms the effectiveness of the L-curve approach for the present case because it almost perfectly corresponds to the noise level added to the temperature signal (σ = 0.1 K).

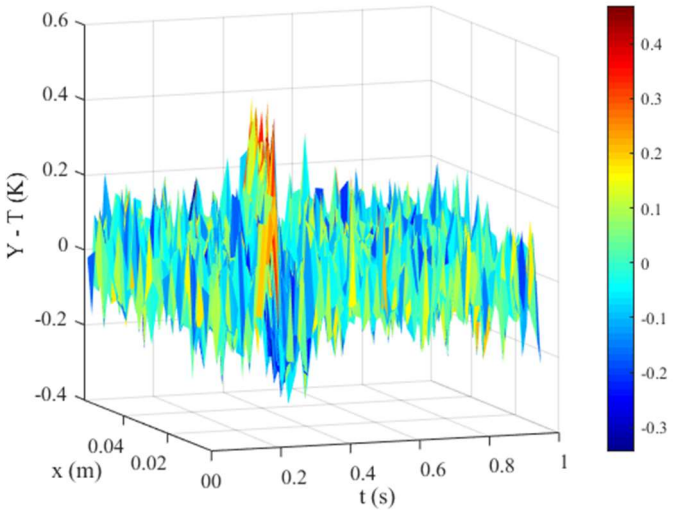

Figure 7. Residuals between experimental and computed temperatures (σ = 0.1 K).

To verify and assess the effectiveness of the adopted solution method at different signal-to-noise levels, an estimation error, described in the following, has been computed:

$$E_h = \frac{\|h_{\text{restored}} - h_{\text{exact}}\|_2}{B \cdot \sqrt{J \cdot N}} \tag{13}$$

Since the noise summed to the temperature distribution significantly rely upon the random arrangement created the procedure to estimate h was repeated for 100 diverse random distributions of noise. Then for each noise level an average value was computed and reported in figure 8.

From figure 8 it is possible to appreciate that the estimation procedure here proposed can restore with a good approximation the h distribution. As highlighted in the introduction, the available attempts of evaluating the local heat transfer coefficient inside mini or micro-channels didn't consider the inverse heat conduction problem approach and made some simplifications. For instance, the heat flux was considered uniformly distributed on the pipe surface and the external pipe wall temperature was used instead of the internal one in Eq. (4).

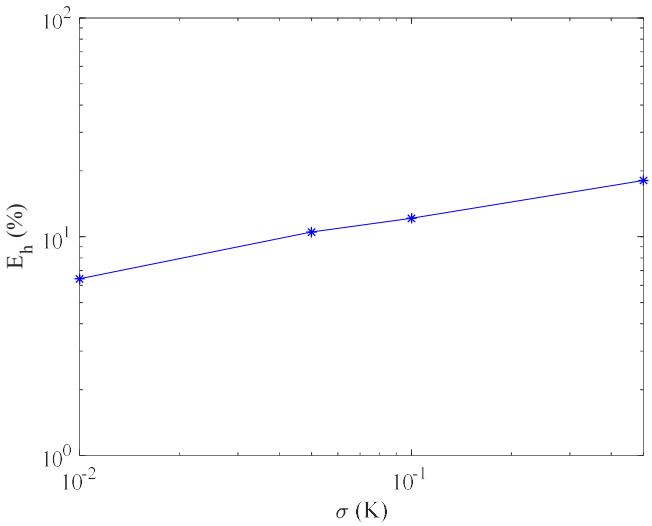

Figure 8. Estimation error on h for various levels of noise.

Due to these assumptions, h can be computed adopting this expression:

$$h_{q_{avg}}(x,t) = \frac{q_{avg}(t)}{T(t,x,r=r_{ext}) - Tb} \tag{14}$$

Under this approach, the heat flux still varies with the time, but it is considered uniform along the axial coordinate. In figure 9 the restored heat transfer coefficient obtained from Eq. (4) and Eq. (14) is reported for the two cases shown in figure 6.

a) b)

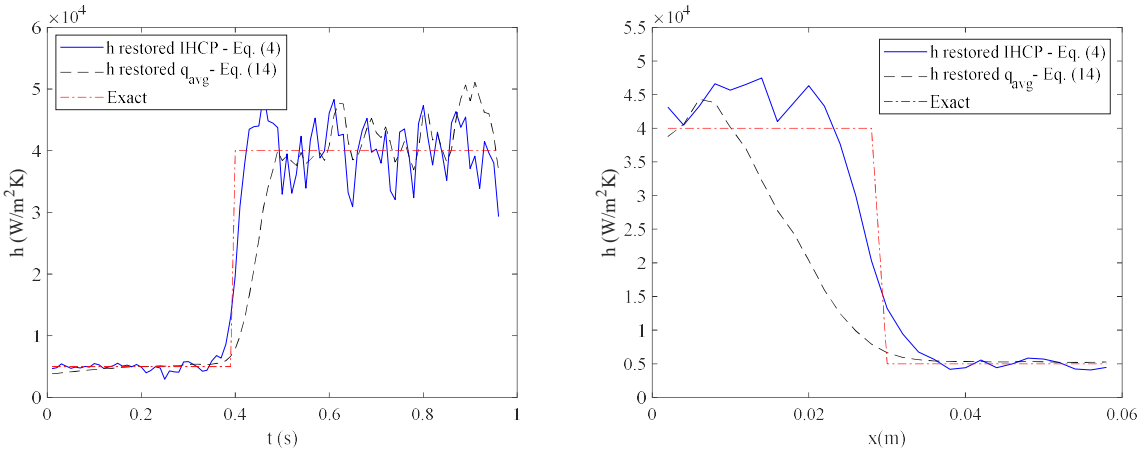

Figure 9. Exact and reconstructed h distribution along axial coordinate (σ = 0.1 K): (a) at x = 0.04; (b) at t = 0.34 s.

It is possible to see that computing the h distribution without IHCP solution in the wall excessively smooth the estimated values, losing some important information. Therefore, the estimation of the local heat flux through the IHCP solution in the pipe wall represents a fundamental step for the final evaluation of the local h distribution.

5. Experimental results

The estimation method previously explained was subsequently adopted for the experimental IR acquisitions. The experimental distribution of temperature measured by the thermographic camera on the outer surface of the capillary copper pipe is shown in figure 10. This temperature distribution was then adopted as entering values in the IHCP approach: specifically, it was considered the evolution in time of the portion of the pipe 0.064 m long that was viewed by the IR camera. It was considered a time interval (1 s) sufficiently extended to guarantee the observation of the crossing of the meniscus along the whole length of the section. The main parameters of the experimental test are gathered in table 3.

Table 3: Experimental test parameters.

q_g (W/m^3)	v_l (m/s)	T_{env} (K)	R_{env} (m^2·K /W)
$1.9 \cdot 10^8$	0.069	295.65	0.1

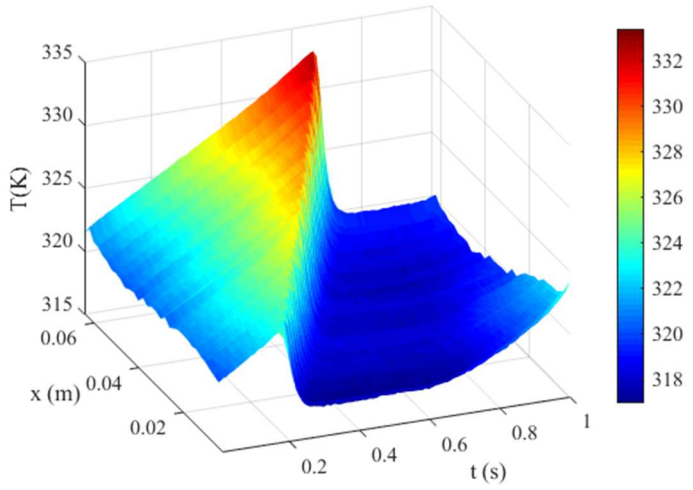

Figure 10. Experimental T distribution on the outer channel surface.

In figure 11a it is reported the external channel wall temperature distribution as a function of time for three x values and in figure 11b the corresponding experimental temperature map for x = 0.034 m.

a) b)

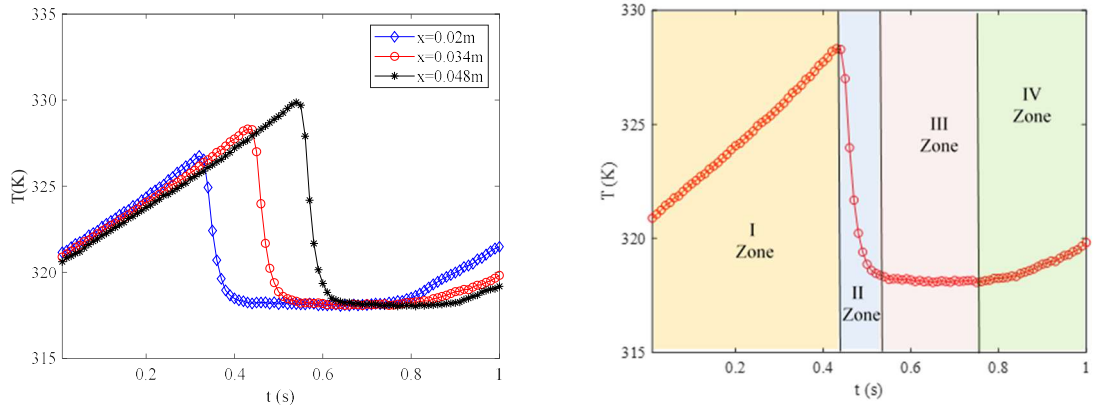

Figure 11. Experimental T distribution on the outer channel wall as a function of time: (a) for three x values and (b) for x = 0.034 m.

The experimental temperature map in figure 10 can be separated in four intervals, relating to diverse heat transfer rates and phenomena in the channel: this is even more clearly visible from figure 11b. The first time interval (zone I) represents the well-known convective cooling in the pipe by liquid laminar flow coupled with the uniform heat generation in the wall by Joule effect [7]; in the second time interval there is the abrupt fall in the temperature distribution corresponding to the crossing of the meniscus (zone II). In the third time interval (zone III) the temperature appears to be practically invariable with time. It corresponds to the thin film evaporation plateau at constant temperature. The last zone (zone IV) represents the steep linear rise of temperature after the end of the thin film evaporation due to dried wall.

Adopting the experimental temperature shown in figure 10, and solving the IHCP in the wall, it is feasible to evaluate the local heat flux at the inner wall-to-fluid interface. The terms $\mathbf{T}_{q=0}$ and $\mathbf{X}$ of Eq. (5) were obtained, as described in Section 4, from the solution of the FEM model realised in Comsol Multiphysics® environment. In the model the global heat-transfer resistance between the outer channel surface and the ambient, R_{env}, was considered equal to 0.1 m^2K/W, that is a typical value when the heat transfer with the ambient is due to the combination of natural convection and radiative processes. The thermal conductivity of the pipe wall was certificated by the producer to be 401 W/m·K; the heat power produced by Joule effect in the pipe q_g was computed dividing the power supplied by the volume of the pipe wall (~$1.9 \cdot 10^8$ W/m^2K, table 3). To establish the value of the regularization factor λ (Eq. (10)), the L-curve method [20], was here applied successfully. The L-curve is presented in figure 12: it shows that an appropriate value of λ could be $2.0 \cdot 10^{-3}$. With this value it was obtained a root mean square residual

of 0.07K that is compatible with the measurements noise achievable with the adopted infrared camera [16].

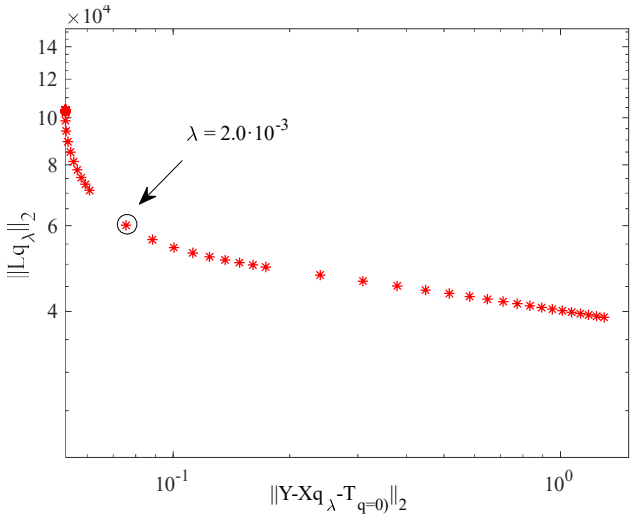

Figure 12. Experimental temperature distribution.

In figures 13, the reconstructed temperature distribution on the outer channel surface for $\lambda = 2.0 \cdot 10^{-3}$ is reported. Figure 14 presents the residuals among the calculated and the experimental temperature for the three abscissa values reported in figure 11a. The fact that the residuals are almost casually dispersed proves that the selected regularization parameter is satisfactory.

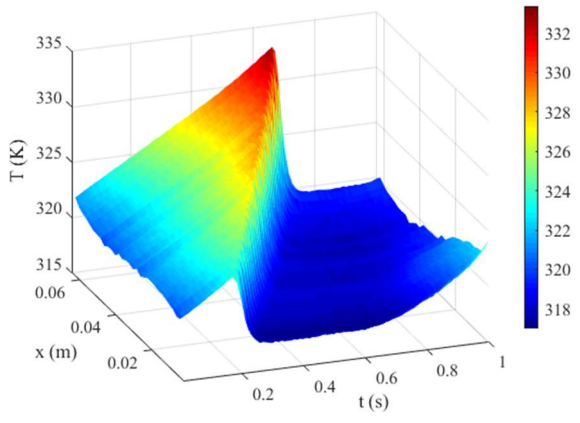

Figure 13. Restored temperature distribution on the external channel wall.

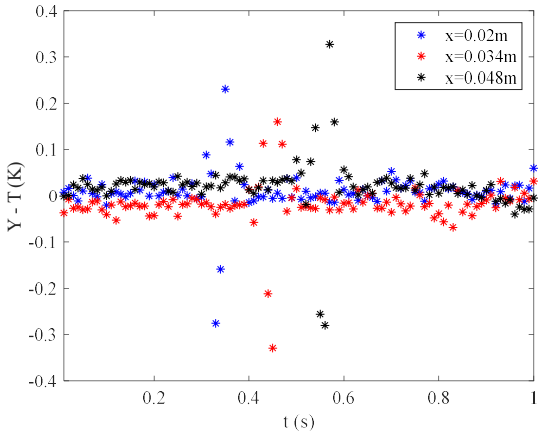

Figure 14. Residuals between the experimental and the computed temperature as a function of time for three abscissae

The local heat flux distribution at the inner channel surface restored by resolving the IHCP is shown in figure 15. The meniscus crossing is evidently perceptible, and it corresponds to the rapid rise of the heat flux: in this zone there is the abrupt vaporization of the film of liquid entrapped among the pipe inner surface and the parabolic shape of the meniscus, and results from the high release of heat from the tube to the fluid, from high to low temperatures (zone II of figure 11b).

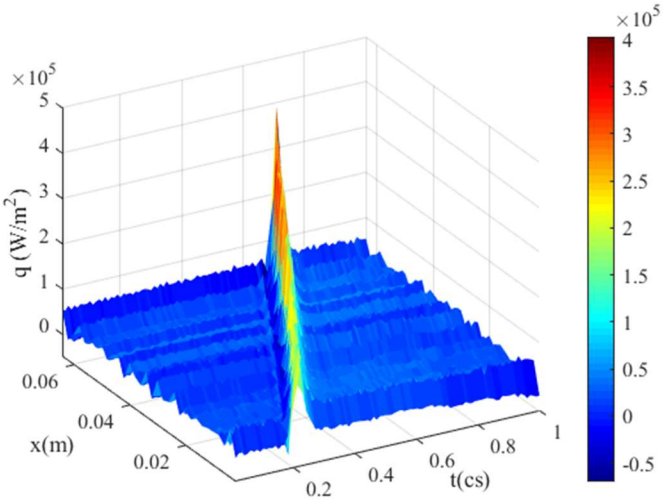

Figure 15. Restored local heat flux distribution at the inner channel surface.

After restoring the heat flux, it is feasible to calculate the local heat transfer coefficient from the ratio between the heat flux and the inner wall to fluid temperature difference. The temperature at the inner surface of the channel (Eq. (4)) was achieved by solving the direct problem applying the restored local heat flux at the inner surface to fluid interface (shown in figure 15).

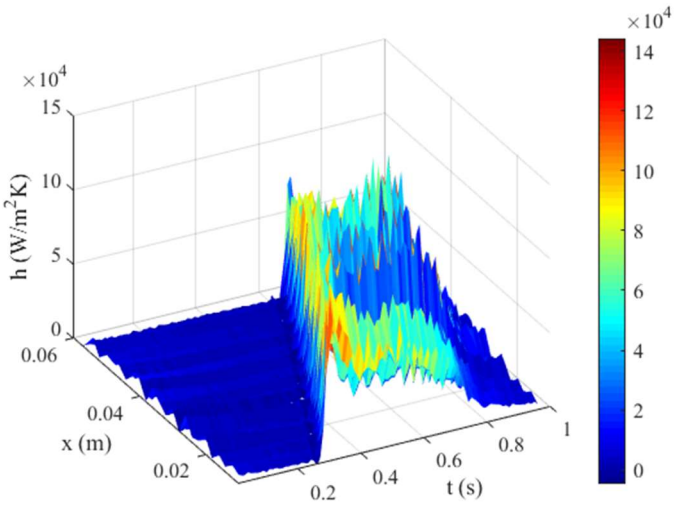

Figure 16. Restored local *h* distribution at the inner channel wall.

The fluid bulk temperature T_b was supposed equivalent to the saturation temperature at the tank (i.e. T_b = 44.25°C), as it was demonstrated in [21]: evaporation takes place at saturation temperature very close to that of the tank, in the range of the measurement error. In figure 16 it is shown the calculated local heat transfer coefficient distribution *h(x,t)*.

It is easily noticeable, in concurrence of the crossing of the meniscus at the vapour–liquid interface, a sudden rise of *h*: in this zone the heat transfer coefficient is at minimum one order of magnitude greater than that occurring for single phase liquid laminar flow.

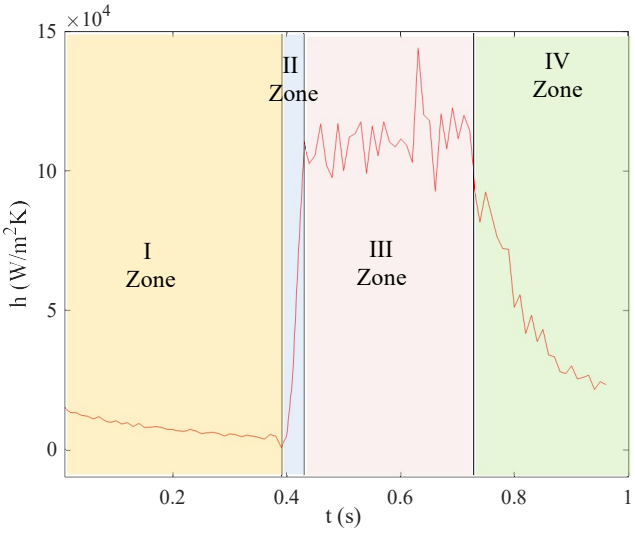

Figure 17. Restored *h* distribution as a function of time for x = 0.034 m.

A more accurate analysis highlights that the restored heat transfer coefficient distribution at one point (x=0.034 m), reported in figure 17 can be separated in four intervals, relating to diverse phenomena and heat transfer rates in the channel.

The first time interval (zone I) represents the well-known convective cooling in the pipe by liquid flow; in the second time interval (zone II) there is the abrupt increase in the heat transfer coefficient correspondent to the crossing of the meniscus and the following deposition of the thin film of liquid on the pipe surface: in this zone there is the sudden evaporation of this thin film. The third time interval (zone III) corresponds to the thin film evaporation and the heat transfer coefficient is characterized by very high and approximately invariant values. The last zone (zone IV) shows the linear decreasing of the heat transfer coefficient due to the increase of dry spots on the tube wall.

The above-described behaviour is clearly shown also in figure 18 where the heat transfer coefficient distribution is reported as a function of time for three different abscissa values. For each x values, it is possible to see both the rapid increase of the *h* values related to the evaporation of thin liquid film and their decrease in the fourth zone due to the fact that the fluid evaporating is always lesser since the main

heat exchange is between the wall and the vapor and it is characterized by lower heat transfer coefficients.

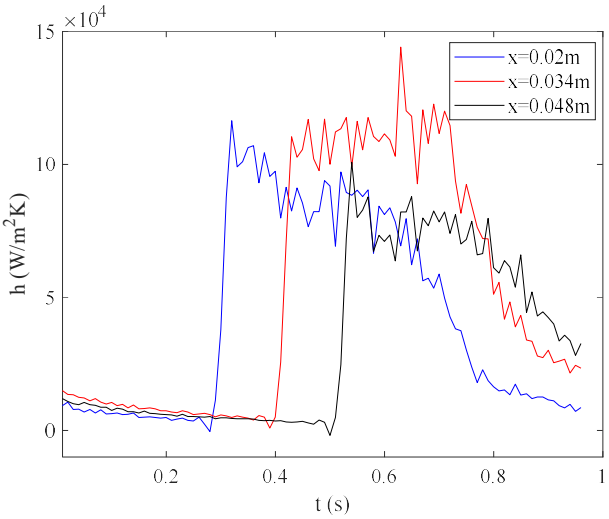

Figure 17. Restored local *h* distribution as a function of time for three abscissae.

From figures 17 and 18 it is possible to obtain useful quantitative information: local *h* can arrive at values up to $1 \cdot 10^5$ W/m^{2}K and presents an average value around $0.8 \cdot 10^5$ W/m^{2}K during the vaporization process of the film deposited at the pipe surface. The outcomes are in satisfying accordance with the results of Thome et al. [5] that studied vaporization in micro-ducts.

Eventually, from Eq. (12) the Nusselt number values were computed. The measured liquid velocity [7] is equal to 0.069 m/s and the corresponding Reynolds number value is 2250. The Nusselt number here experimentally determined for the previous liquid phase (Nu ≈ 15) is in good agreement with the experimental findings of Adams et al. [22] and Wu et al. [23] for single-phase liquid flow in mini and micro-channels that for a similar case indicated a Nusselt number in the range 10-25.

Regarding the Nusselt number in the area in which film evaporation occurs, it was found to be around 350, that means significantly higher than the usual values found for average Nusselt number for flow boiling phenomena in mini or micro-channels [24].

6. Conclusions

In the here presented research the main objective was the experimental estimation of the local heat flux and convective heat transfer coefficient inside a capillary copper tube in case of vaporization of a thin film of liquid deposited on the inner wall of the pipe. To reach this goal an inverse estimation procedure was adopted on the temperature maps acquired on the external surface of the channel thanks to a thermographic camera.

Before applying the proposed solution technique to experimental data, it was used to retrieve the local heat transfer coefficient in case of synthetic data spoiled with random noise. The outcomes of the numerical validation demonstrated the satisfying performance of the proposed estimation method by highlighting its ability to restore the required physical quantities at different levels of noise.

Once validated, the approach was adopted to estimate the local heat transfer coefficient distribution for the experimental case of a semi-infinite slug flow in a pipe with uniform heat generation in the wall by Joule effect.

From the experimental investigation it was possible to determine, during the crossing of the meniscus that separate the liquid slug from the vapor plug, four different areas characterized by diverse heat transfer rates and phenomena in the channel. After the first zone where the convective cooling occurred in the pipe by liquid laminar flow, a second zone is observed, and it was characterized by the sudden rise in the heat transfer coefficient value. It corresponded to the passage of the meniscus that is followed by a time interval where the thin film evaporation arose: the heat transfer coefficient was characterized by very high values and the wall temperature is almost constant. On quantitative point of view the local h reached values up to $1 \cdot 10^5$ MW/m^{2}K and showed an average value around $0.8 \cdot 10^5$ W/m^{2}K during this third phase. Also, the Nusselt number was computed and presented values significantly higher than the usual ones for flow boiling phenomena in mini or micro-channels. In the last zone it was possible to detect a linear decreasing of the heat transfer coefficient due to the increase of dry spots on the tube wall.

This detailed observation of a semi-infinite slug flow in a capillary tube is, without a doubt, original. Moreover, a further significant result of the present work is the presented estimation procedure that could be profitably utilized in many different other cases of two-phase heat transfer devices to obtain the optimization of their performances.

Acknowledgments

The Authors would like to acknowledge the European Space Agency (ESA) support through the grant 4000128640/19/NL/PG/pt, ESA MAP project TOPDESS.

Nomenclature

Symbol	Quantity	SI Unit
c_p	Specific heat	J/kg·K
D	Diameter	m
h	Convective heat-transfer coefficient	W/m^2·K
L	Derivative operator	

k	Thermal conductivity	W/m·K
Nu	Nusselt number	-
q	Convective heat flux	W/m^2
$\mathbf{q}$	Convective heat-flux vector	W/m^2
q_g	Internal heat generation per unit volume	W/m^3
r	Radial coordinate	m
R_{env}	Overall heat-transfer resistance between the tube wall and the surrounding environment	$m^2 \cdot K/W$
T	Temperature	K
$\mathbf{T}$	Estimated temperature vector	K
x	Axial coordinate	m
$\mathbf{X}$	Sensitivity matrix	$m^2 \cdot K/W$
$\mathbf{Y}$	Measured temperature vector	K

Greeks

δ	Liquid film thickness	m
λ	Regularization parameter	
ρ	Density	Kg/m^3

Subscripts

avg	average
b	Bulk
env	Environment
ext	External
f	Fluid
int	Internal

References

[1] Murshed S S and De Castro C N 2017 A critical review of traditional and emerging techniques and fluids for electronics cooling Renew. Sust. Energ. Rev. **78** 821.

[2] Pua L M and Rumbold S O 2003 Industrial Microchannels Devices: Where Are We Today?, Proc. of 1st Int. Conf. on Microchannels and Minichannels, Rochester, New York, USA.

[3] J.R. Thome, M. Groll, R. Mertz, Section 2.13.4 Microscale Heat Transfer: Boiling and Evaporation in Chapter 2.13 Heat Transfer and Fluid Flow in Microchannels, Heat Exchanger Design Update, Begell House, New York, 2.13.4.1-27, 2003.

[4] S.G. Kandlikar, Two-phase flow patterns, pressure drop and heat transfer during boiling in minichannel and microchannel flow passages of compact heat exchangers, in: Compact Heat Exchangers and Enhancement Technology for the Process Industries, Begell House, New York, 2001, pp. 319–334.

[5] A.E. Bergles, V.J.H. Lienhard, G.E. Kendall, P. Griffith, Boiling and evaporation in small diameter channels, Heat Transfer Eng. 24 (2003) 18–40

[6] A.M. Jacobi, J.R. Thome, Heat transfer model for evaporation of elongated bubble flows in microchannels, J. Heat Transfer 124 (2002) 1131–1136.

[7] Chauris N, Ayel V, Bertin Y and Romestant C 2015. Evaporation of a liquid film deposited on a capillary heated tube: Experimental analysis by infrared thermography of its thermal footprint *Int J Heat Mass Tran* **86** 492.

[8] Thome J R, Dupont V, Jacobi A M 2004 Heat transfer model for evaporation in microchannels. Part I: presentation of the model *Int J Heat Mass Tran* **47** 3375.

[9] Kandlikar, S. G. (2002). Fundamental issues related to flow boiling in minichannels and microchannels. Experimental Thermal and Fluid Science, 26(2-4), 389-407.

[10] Khandekar, S., Schneider, S. M., Schäfer, P., Kulenovic, R., Groll, M., Thermofluid dynamic study of flat-plate cosed-loop Pulsating Heat Pipes, Microsc. Thermophys. Eng. 6 (2002) 303–317.

[11] Khandekar, S., Panighahi, P.-K., Lefèvre, F., Bonjour, J., Local hydrodynamic of flow in a Pulsating Heat Pipe: a review, Fr. Heat Pipes 1 (2010) 1–20.

[12] Bozzoli F, Cattani L, Rainieri S, Bazan F S V, Borges L S (2014) Estimation of the local heat transfer coefficient in the laminar flow regime in coiled tubes by the Tikhonov regularisation method Int. J. Heat Mass Transf. 72 352–361.

[13] Sun, Y., Guo, C., Jiang, Y., Wang, T., & Zhang, L. (2018). Transient film thickness and microscale heat transfer during flow boiling in microchannels. International Journal of Heat and Mass Transfer, 116, 458-470.

[14] Yan, Y. Y., & Lin, T. F. (1998). Evaporation heat transfer and pressure drop of refrigerant R-134a in a small pipe. International Journal of Heat and Mass Transfer, 41(24), 4183-4194.

[15] Maciejewska, B., & Piasecka, M. (2019). Time-dependent study of boiling heat transfer coefficient in a vertical minichannel. International Journal of Numerical Methods for Heat & Fluid Flow.

[16] Bozzoli, F., Cattani, L., Mocerino, A., & Rainieri, S. (2018). Turbulent flow regime in coiled tubes: local heat-transfer coefficient. Heat and Mass Transfer, 54(8), 2371-2381.

[17] Beck J V, Blackwell B, St Clair C R Jr 1985 *Inverse Heat Conduction: Ill-Posed Problems* A Wiley-Interscience (New York).

[18] Tikhonov A N, Arsenin V I and John F 1977 *Solutions of ill-posed problems* (Washington DC: Winston).

[19] Najafi H, Woodbury K A, Beck J V 2015 Real time solution for inverse heat conduction problems in a two-dimensional plate with multiple heat fluxes at the surface, *Int. J. Heat Mass Transfer* **91** 1148–1156.

[20] Hansen P C 1990 Truncated singular value decomposition solutions to discrete illposed problems with ill-determined numerical rank *SIAM J. Sci. Stat. Comput.* **11** 503–518.

[21] Ayel V., Bertossi R., Mehta B., Chauris N., Romestant C., Bertin Y., Evaporation of a thin liquid film in a heated capillary tube: experimental results and discussion on the related physical phenomena, IX Minsk Int. Seminar: "Heat Pipes, Heat Pumps, Refrigerators, Power Sources", Minsk, Belarus, 07-10 September, 2015.

[22] T. M. Adams, S. M. Abdel-Khalik, S. M. Jeter, and Z. H. Qureshi, An Experimental Investigation of Single-Phase Forced Convection in Microchannels, Int. J. Heat Mass Transfer, vol. 41, no. 6–7, pp. 851–857, 1998.

[23] P. Wu and W. A. Little, Measurement of Heat Transfer Characteristics of Gas Flow in Fine Channel Heat Exchangers Used for Microminiature Refrigerators, Cryogenics, vol. 24, no. 8, pp. 415–420, 1984.

[24] Mahmoud, M. M., & Karayiannis, T. G. (2013). Heat transfer correlation for flow boiling in small to micro tubes. International Journal of Heat and Mass Transfer, 66, 553-574.